

# A generating mechanism for apparent fluid slip in hydrophobic microchannels

Derek C. Tretheway and Carl D. Meinhart<sup>a)</sup>

*Department of Mechanical Engineering, University of California, Santa Barbara, California 93106*

(Received 27 August 2003; accepted 14 January 2004; published online 5 April 2004)

Fluid slip has been observed experimentally in micro- and nanoscale flow devices by several investigators [e.g., Tretheway and Meinhart, *Phys. Fluids* **14**, L9 (2002); Zhu and Granick, *Phys. Rev. Lett.* **87**, 096105 (2001); Pit *et al.*, *Phys. Rev. Lett.* **85**, 980 (2000); and Choi *et al.*, *Phys. Fluids* **15**, 2897 (2003)]. This paper examines a possible mechanism for the measured fluid slip, for water flowing over a hydrophobic surface. We extend the work of Lum *et al.* [*J. Phys. Chem. B* **103**, 4570 (1999)], Zhu and Granick [*Phys. Rev. Lett.* **87**, 096105 (2001)], Granick *et al.* [*Nature Materials* **2**, 221 (2003)], and de Gennes [*Langmuir* **18**, 3413 (2002)], who suggest slip develops from a depleted water region or vapor layer near a hydrophobic surface. By modeling the presence of either a depleted water layer or nanobubbles as an effective air gap at the wall, we calculate slip lengths for flow between two infinite parallel plates. The calculated slip lengths are consistent with experimental values when the gas layer is modeled as a continuum and significantly higher when rarefied gas conditions are assumed. The results suggest that the apparent fluid slip observed experimentally at hydrophobic surfaces may arise from either the presence of nanobubbles or a layer of low density fluid at the surface. © 2004 American Institute of Physics. [DOI: 10.1063/1.1669400]

## I. INTRODUCTION

The current development of microfluidic devices for micro-total analysis systems has led to research focused on fluid flow at the microscale. Since the surface to volume ratio depends inversely on the characteristic length scale, the importance of boundary conditions increases as the dimensions of microfluidic devices decrease. For nearly a hundred years, scientists and engineers have assumed no slip for fluid flow over a solid surface. While this assumption has been proven experimentally at the macroscale, recent experiments with micro- and nanoscale flows indicate the proper boundary condition depends both on the characteristic length scale of the flow and the chemical and physical properties of the solid surface.

Ruckenstein and Rajora<sup>1</sup> investigated fluid slip in glass capillaries with surfaces made repellent to the flowing liquid. Their experimental results of pressure drop indicate larger slip than that predicted by chemical potential theory, where slip is proportional to the gradient in the chemical potential. The results suggest that slip occurs over a gap near the surface rather than directly on the solid surface, and the gap forms when a hydrophobic liquid flows over a hydrophilic surface, and vice versa. They suggest the gap may be increased in thickness by the release of gases entrained in the flowing liquid and/or the desorption of soluble gases. Their results, however, are inferred from pressure drop versus flow rate measurements and are not a direct measurement of the fluid velocity.

Computationally, Barrat and Bocquet<sup>2</sup> predict slip in na-

noporous medium when the liquid is sufficiently nonwetting, which increases the effective permeability of the nanoporous medium. Their predictions are experimentally justified by Churaev *et al.*,<sup>3</sup> who postulated slip at the wall to recover the viscosity of water for water flow in thin ( $<1 \mu\text{m}$ ) hydrophobic capillaries.

Pit *et al.*<sup>4</sup> observe fluid slip for hexadecane between two rotating parallel disks with a gap of 190 microns. By following the movement of a photo-bleached test section, they measure no slip when the surfaces are coated with perfluorodecanetrichlorosilane, a slip length of approximately 170 nm for bare sapphire, and a slip length of 400 nm for an octadecyltrichlorosilane (OTS) coating. They conclude that slip depends on both the interfacial energy and surface roughness.

At a much smaller length scale, Craig *et al.*<sup>5</sup> calculate the drainage force for a sphere approaching a solid, flat wall. They measure slip lengths up to 20 nm for aqueous sucrose solutions that have advancing and receding contact angles of 70 and 40 degrees, respectively. They conclude that the slip length depends nonlinearly on the approach rate of the sphere.

Zhu and Granick<sup>6</sup> experimentally observe fluid slip in an oscillating surface force apparatus. For cylinder separations from approximately 10–200 nm, they measure slip lengths (point into the wall at which the inferred velocity would go to zero) of up to  $2.5 \mu\text{m}$  for water between octadecyltriethoxysilane (OTE) surfaces,  $1.5 \mu\text{m}$  for tetradecane between OTE surfaces, and  $0.9 \mu\text{m}$  for tetradecane between mica surfaces. Their results suggest a strong dependence between the velocity gradient and magnitude of the slip, a critical shear rate for onset of fluid slip, and an increase in the slip length as the separation between the cylinders decreases.

<sup>a)</sup> Author to whom correspondence should be addressed. Electronic mail: meinhart@engineering.ucsb.edu

Their conclusions, however, are inferred from discrepancies between the measured normal force and expected normal force assuming no slip. More recently, Zhu and Granick<sup>7</sup> examine the relative importance of surface roughness and fluid–surface interactions in determining the appropriate boundary condition. For similar, poorly wetting surfaces, the critical shear rate to observe deviations from force predictions assuming no slip increased nearly exponentially with increasing surface roughness. They conclude that local intermolecular interactions dominate when surfaces are very smooth, but are otherwise negligible for sufficient surface roughness.

Tretheway and Meinhart<sup>8</sup> measured fluid velocities in hydrophilic and hydrophobic microchannels by micron resolution particle image velocimetry ( $\mu$ -PIV). The results showed a significant fluid velocity near a hydrophobic microchannel wall and no-slip for a hydrophilic surface. A slip length of 0.92 microns was estimated.

Choi *et al.*<sup>9</sup> measured the pressure drop for flow through hydrophobic and hydrophilic microchannels. From discrepancies with the expected pressure drop, slip lengths of order tens of nanometers were calculated for both hydrophilic and hydrophobic surfaces, with hydrophobic surfaces having slightly larger slip lengths.

While observations of fluid slip continue to expand, the generating mechanism responsible for fluid slip is not well understood. Recently, nanobubbles on hydrophobic surfaces were observed experimentally by Tyrell and Attard<sup>10</sup> and Steitz *et al.*<sup>11</sup> With atomic force microscopy, Tryell and Attard<sup>10</sup> measured pancake-shaped nanobubbles with heights between 10 and 30 nanometers with a much larger lateral extent. This relatively flat shape reduces the effective curvature of the nanobubbles such that the internal pressure is significantly reduced compared to the 140 atmospheres expected for a spherical 10 nm nanobubble. Lum *et al.*<sup>12</sup> and others<sup>11,13,14</sup> suggest a depleted water region or vapor layer develops for water near a hydrophobic surface. Zhu and Granick<sup>6</sup> indicate that the calculated slip lengths at higher shear rates are consistent with a two-layer fluid model with a lower viscosity layer near the surface. However, a detailed characterization is not provided. More recently, Granick *et al.*<sup>15</sup> saturated tetradecane with carbon dioxide and argon and calculated the slip in a surface force apparatus with a mica and a partially wetting methyl-terminated surface. They observe no-slip behavior when tetradecane is saturated with carbon dioxide, while massive deviations from the no-slip prediction exists for tetradecane saturated with argon. They attribute this difference to the enhanced segregation of argon with the amount of segregation dependent on the material properties of the fluid, the chemical nature of the wall, and chemical identity of the dissolved gases. This is within the context of dissolved gases forming a vapor layer or low-density region near the surface. De Gennes<sup>16</sup> examined a two-layer fluid model with a gas film in the Knudsen regime. With rarefied conditions, de Gennes<sup>16</sup> predicts a slip length that is independent of gas thickness and with relatively large values. For typical conditions, a slip length equal to 7  $\mu\text{m}$  is obtained.

The current work examines a possible mechanism for the

apparent fluid slip by modeling the presence of either nanobubbles or a depleted water region as an effective air gap at the wall (an idealized case for either nanobubbles or a depleted layer). We calculate slip lengths for flow between two infinite parallel plates, which are consistent with various experimental values. This suggests that the apparent fluid slip observed experimentally arises from either nanobubbles or a thin-low viscosity layer at the hydrophobic surface.

## II. VELOCITY PROFILES NEAR A MICROCHANNEL WALL

### A. Experimental system

Tretheway and Meinhart<sup>8</sup> measured fluid motion through a 30 $\times$ 300 micron channel by micron-resolution particle image velocimetry ( $\mu$ -PIV). Details of the experiments are described in Tretheway and Meinhart.<sup>8</sup> The interrogation region was 128 $\times$ 8 pixels, which yields a spatial resolution of 14.7  $\mu\text{m}$  in the streamwise direction, 900 nm in the spanwise direction, and 1.8  $\mu\text{m}$  in depth. With a 50% overlap of interrogation regions, they obtained velocity measurements to within 450 nm of the channel wall. To increase the signal to noise ratio, 48 image pairs were cross correlated and the resulting correlations were ensemble averaged (Meinhart *et al.*<sup>17</sup>). The 30  $\mu\text{m}$  deep by 300  $\mu\text{m}$  wide extruded glass microchannels were trimmed to a length of approximately 8 cm. Deionized water seeded with the 300 nm diameter fluorescent polystyrene spheres (Interfacial Dynamics Corporation) was injected through tubing attached to the capillary tube into the microchannel by a gravity feed system. The flow rate was constant at approximately 200  $\mu\text{l/h}$ . Measurements were taken in the midplane of the channel (15  $\mu\text{m}$  from the bottom) near the side wall at a distance 4 to 4.5 cm from the entrance of the microchannel. This ensured a fully developed flow profile. Differences in the boundary conditions are determined by comparing the velocity profiles between hydrophilic and hydrophobic microchannels. An untreated glass microchannel is naturally hydrophilic. Hydrophobic microchannels were created by coating the walls of the microchannel with octadecyltrichlorosilane (OTS). At maximum density, the OTS layer is approximately 23 angstroms thick with a surface roughness of 2–3  $\text{\AA}$ . As the contact angle cannot be measured inside the microchannel, a reference section of glass was treated concurrently with the microchannels to provide an estimate of the effectiveness of the reaction. Contact angles for water of approximately 120 $^\circ$  were measured, which is consistent with previously measured contact angles of OTS.

### B. Results

From Tretheway and Meinhart,<sup>8</sup> Fig. 1 shows the average velocity profiles for flow near hydrophilic (squares) and hydrophobic (triangles) microchannel surfaces. The velocity is normalized with the free-stream velocity. For a hydrophilic microchannel, the velocity is near its free-stream value at 25 microns and smoothly decreases to zero near the wall. This profile agrees within 2% of the analytical solution for flow through a rectangular channel with a finite aspect ratio. This

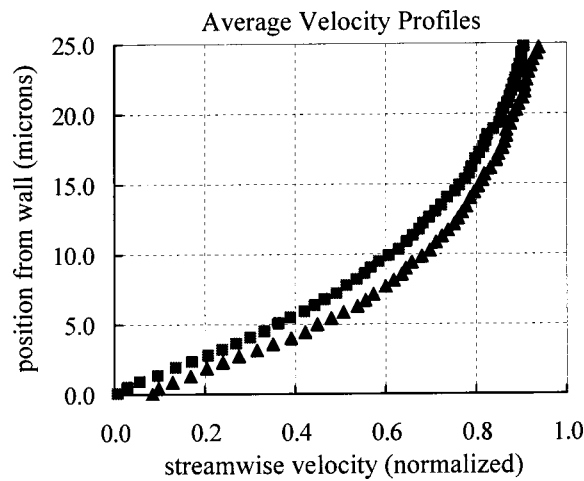


FIG. 1. Velocity profiles for flow over a hydrophilic (square) and hydrophobic (triangle) microchannel surface. The velocity profiles are normalized by the free-stream velocity (reproduced from Tretheway and Meinhart, Ref. 8).

indicates that the no-slip boundary condition is valid for water flowing over a hydrophilic surface, and that the micro-PIV technique accurately measures the no-slip boundary condition. For flow through a hydrophobic microchannel, the velocity profile is significantly different. Figure 1 shows the hydrophobic velocity profile (triangles) near its free-stream value at  $25 \mu\text{m}$  and decreasing towards the wall, with a finite and significant velocity measured within  $450 \text{ nm}$  above the wall. This slip velocity is approximately 9% of the free-stream velocity. From the measured shear rate at the wall, the calculated slip length equals  $0.92 \text{ microns}$ . This slip length is consistent with the measured slip lengths of Zhu and Granick<sup>6</sup> and Pit *et al.*<sup>4</sup>

### III. MECHANISMS FOR APPARENT FLUID SLIP

The mechanism for the generation of the apparent fluid slip is unknown. Ruckenstein and Rajora<sup>1</sup> suggest that fluid slip may develop from entrained and soluble gases forming a gap near the wall. Recently, Tyrell and Attard<sup>10</sup> imaged, with an atomic force microscope, a hydrophobic glass surface submerged in water. Their results showed the presence of pancake-shaped, 20 to 30 nm thick nanobubbles completely covering the surface. In addition, they showed that the hydrophobic surface acts as a nucleation site pulling dissolved gases out of solution. Within 10 to 20 min after scraping the surface clean, the surface was once again completely covered with nanobubbles.

Lum *et al.*<sup>12</sup> and others<sup>11,13,14</sup> suggest that a depleted water region or vapor layer exists near a hydrophobic surface in contact with water. This depleted region develops regardless of the presence of dissolved or entrained gases and may act as a precursor to nanobubbles observed by Tyrell and Attard<sup>10</sup> and Steitz *et al.*<sup>11</sup>

In Tretheway and Meinhart,<sup>8</sup> velocity measurements were made for deionized water flowing over a hydrophobic surface. No treatment of the water was conducted to remove dissolved or entrained gases. In order to determine if either dissolved gases or a depleted region could generate the ap-

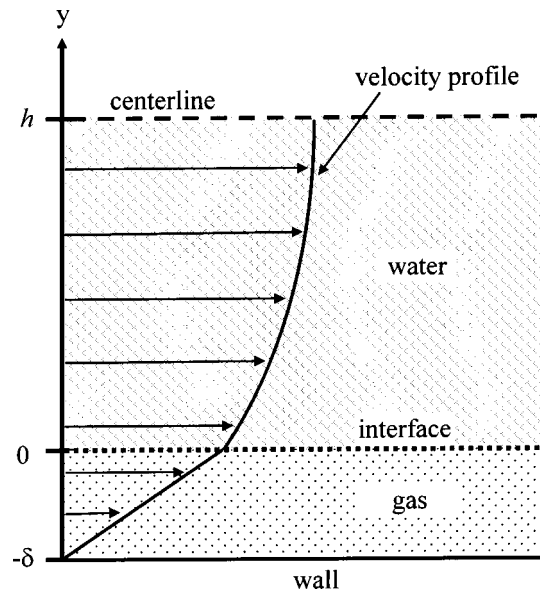


FIG. 2. The physical model of fluid distribution between two infinite parallel plates (schematic). Gas layer of thickness  $\delta$  near the walls and a plate separation of  $2h$ .

parent fluid slip in Fig. 1, we examine analytically flow between two infinite parallel plates, assuming nanobubbles or a depleted region form an effective air gap near the wall. Figure 2 provides a schematic of the physical model. From this simple one-dimensional model we can calculate the bubble height or air gap required to generate measured slip lengths, assuming Navier's hypothesis effectively describes a thin air gap at the surface. Navier's hypothesis states that the velocity at a surface is proportional to the shear rate at the surface

$$u(y=0) = \beta \left. \frac{du}{dy} \right|_{y=0}, \quad (1)$$

where  $\beta$  has units of length and is defined as the slip length.

#### A. Air gap with a continuum approximation

For two-phase flow between two infinite parallel plates with a thin air gap of thickness,  $\delta$ , at the wall and a fluid layer of thickness  $2h$ , the solution for the velocity in the water phase assuming Stokes flow for both phases, no stress at the centerline, continuity of stress and velocity at the air-water interface, and no-slip at the air-wall interface is

$$u = \frac{1}{2\mu_w} \left( \frac{dp}{dx} \right) \left[ y^2 - 2hy - 2 \frac{\mu_w}{\mu_a} h \delta - \frac{\mu_w}{\mu_a} \delta^2 \right], \quad (2)$$

where  $\mu_a$  and  $\mu_w$  are the viscosity of air and water, respectively,  $(-dp/dx)$  is the pressure drop,  $y=0$  at the air-water interface, and  $y=-\delta$  at the wall. Assuming Navier's hypothesis effectively describes the thin air gap at the wall, we set the velocity at the air-water interface equal to the slip length times the shear rate at the air-water interface and obtain an equation for the slip length as a function of the air gap thickness and the plate separation

$$\beta_{\text{cont.}} = \frac{\mu_w}{\mu_a} \left( \frac{\delta^2}{2h} + \delta \right). \quad (3)$$

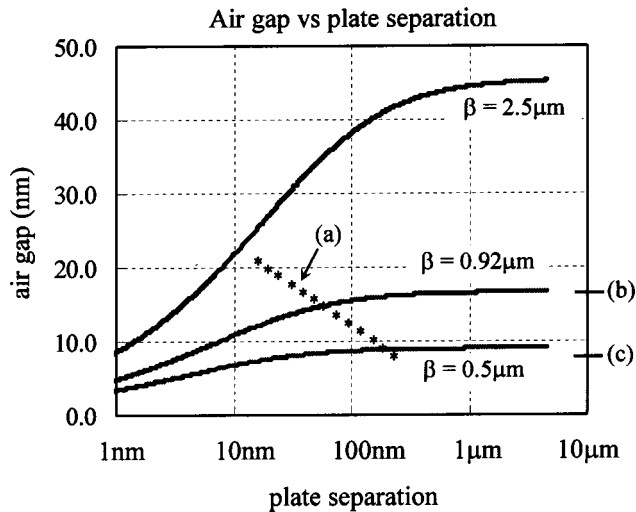


FIG. 3. Air gap thickness as a function of plate separation to produce a given slip length. Locations of experimentally measured slip lengths indicated. (a) Zhu and Granick (Ref. 6); (b) Tretheway and Meinhart (Ref. 8); and (c) Pit *et al.* (Ref. 4). Tyrell and Attard (Ref. 10) measured nanobubble heights of 20–30 nm.

Figure 3 shows the air gap thickness required for a given plate separation to generate a particular slip length. We assume standard conditions for air and water at 20 °C ( $\mu_w = 1.0019$  cp,  $\mu_a = 0.0183$  cp). As the plate separation decreases, the slip length generated by a fixed air gap thickness increases. At very small separations, the slip length is strongly dependent on the air gap thickness. Tretheway and Meinhart<sup>8</sup> report a slip length of  $\beta = 0.92 \mu\text{m}$ . With 30  $\mu\text{m}$  channels, this yields a required air gap thickness of approximately  $\delta = 18$  nm. This thickness is consistent with the measured bubble heights of Tyrell and Attard.<sup>10</sup> In addition, when surfaces are hydrophobic, Zhu and Granick<sup>6</sup> calculated slip lengths of approximately  $\beta = 2.5 \mu\text{m}$  for a  $2h = 20$  nm separation. The corresponding bubble height of  $\delta \sim 20$  nm is consistent with the required bubble height in this work and the measured values of Tyrell and Attard.<sup>10</sup> However, as shown in Fig. 3, Zhu and Granick<sup>6</sup> reported a range of slip lengths with smaller slip lengths at larger separations. This yields a range of bubble heights from approximately  $\delta = 8$  to 20 nm for separations from 300 to 20 nm. Pit *et al.*<sup>4</sup> calculate a slip length of approximately  $\beta = 400$  nm for a  $2h = 190 \mu\text{m}$  separation, which would require a bubble height of  $\delta = 9$  nm. These results suggest that an effective air gap at hydrophobic surfaces could explain some of the experimental observations of fluid slip. However, the above results must be used with caution. Because the bubble heights are of order of tens of nanometers, the gas phase being a continuum is a strong idealization.

### B. Air gap with rarefied gas conditions

According to the above calculations, the air gap/bubble heights required to generate the measured slip length are tens of nanometers. The characteristic Knudsen number,  $\text{Kn} = \lambda/\delta$ , therefore is large, which suggests that the gas phase is not a continuum. Thus, the assumption of no slip at the air–

wall interface is not strictly valid. A more reasonable boundary condition may be obtained from the kinetic theory of gases.<sup>18</sup> For rarefied conditions, where the length scale is less than the mean free path of the gas, the boundary condition for a gas at a solid wall is

$$u_{\text{rare}}(y = -\delta) = \left(\frac{2-\sigma}{\sigma}\right) \left(\frac{2}{3}\lambda\right) \left(\frac{du}{dy}\right)_{y=-\delta} = \varepsilon \left(\frac{du}{dy}\right)_{y=-\delta}, \quad (4)$$

where  $\lambda$  is the mean free path of the gas and  $\sigma$  is the accommodation coefficient.<sup>18</sup> For diatomic molecules the mean free path is roughly 100 nm. The accommodation coefficient equals 1 when all molecules are reflected diffusely and equals zero when specularly reflected (i.e., perfect slip). Solving two-phase flow between two infinite parallel plates as described in the previous section, but with the no-slip air–wall boundary condition replaced with Eq. (4), yields the equation for the velocity in the water phase

$$u_{\text{rare}} = \left(\frac{-dp}{dx}\right) \left[ -\frac{y^2}{2\mu_w} + \frac{hy}{2\mu_w} + \frac{1}{\mu_a} \left( \varepsilon\delta + \frac{\delta^2}{2} + (\varepsilon + \beta)h \right) \right], \quad (5)$$

where  $(-dp/dx)$  is the pressure drop,  $\mu_w$  and  $\mu_a$  are the water and air viscosities, respectively,  $\delta$  is the thickness of the air gap/bubble height,  $h$  is the plate separation, and  $\varepsilon$  is defined in Eq. (4). Assuming Navier's hypothesis effectively describes the thin air gap at the wall, we set the velocity at the air–water interface equal to the slip length times the shear rate at the air–water interface and obtain an equation for the slip length as a function of plate separation and the air gap thickness

$$\beta_{\text{rare}} = \frac{1}{2h} \left(\frac{\mu_w}{\mu_a}\right) [\delta^2 + 2(\varepsilon + h)\delta + 2\varepsilon h]. \quad (6)$$

It is obvious from Eq. (6) when compared to Eq. (3) that the apparent fluid slip is greatly enhanced for a rarefied gas. From Eq. (6) we can calculate the expected slip length for the experimental conditions of Tretheway and Meinhart.<sup>8</sup> We assume standard conditions for air and water at 20 °C ( $\mu_w = 1.0019$  cp,  $\mu_a = 0.0183$  cp), a mean free path equal to 100 nm, and an accommodation coefficient equal to 1, which is generally a good approximation<sup>18</sup> and provides a lower limit of slip at the gas–wall interface. Figure 4 shows the slip length increases dramatically with increasing thickness. Assuming an air gap thickness equal to 20 nm (the approximate bubble height measured by Tyrell and Attard<sup>10</sup>), the calculated slip length equals  $\beta = 4.79 \mu\text{m}$ . This calculated slip length is considerably larger than the measured slip length of  $\beta = 0.92 \mu\text{m}$ . Interestingly, below approximately  $\delta = 10$  nm the calculated slip length has a nearly constant value,  $\beta = 3.68 \mu\text{m}$ . Thus, even if we assume the smallest possible air gap, the rarefied gas conditions (slip at the air–wall interface) produces a slip substantially larger than any experimental estimated slip lengths. The relatively large slip length, 3.68  $\mu\text{m}$  minimum, is consistent with that of de Gennes,<sup>16</sup> who calculated a 7  $\mu\text{m}$  slip length for a two-layer

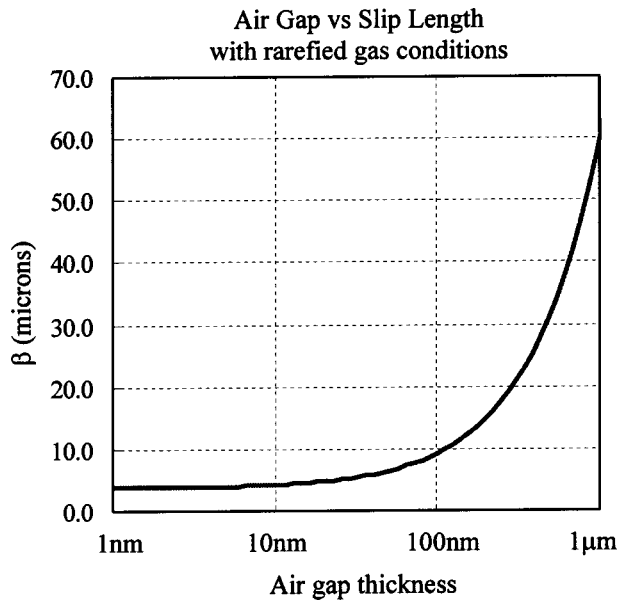


FIG. 4. Air gap versus slip length with rarefied gas conditions in air gap assuming  $\lambda=100$  nm,  $h=30$   $\mu$ m, and standard conditions for air and water at 20 °C.

fluid model with a gas phase in the Knudsen regime. Thus, rarefied gas conditions produce significantly large slip lengths. In addition, de Gennes<sup>16</sup> shows that the slip length is, for practical purposes, independent of the gas phase thickness. For small air gaps ( $\delta < 10$  nm), Fig. 4 shows a nearly constant slip length. However, for air gaps greater than 10 nm, the slip length increases as the air gap increases. At 100 nm (the value of the mean free path) the slip length,  $\beta$ , is approximately 2.5 times the slip length at 10 nm. While a discrepancy in the behavior of the slip length on air gap thickness exists, the values of the slip lengths are quite similar.

The idealized physical model overestimates the slip length for the presence of a continuous gas layer. The relatively large slip lengths may arise either from our assumption of the physical properties of the depleted layer or from our assumption that the surface is covered uniformly by a gas layer (i.e., continuous nanobubble coverage). For example, we assume standard atmospheric properties for the gas layer and a mean free path equal to 100 nm. These assumptions may be quite crude as the actual pressure inside the nanobubble or depleted region may be significantly higher. An increase in pressure would reduce the calculated slip lengths by increasing the effective viscosity and decreasing the mean free path. The assumption of continuous bubble coverage is addressed in the next section.

### C. Intermittent surface coverage

The previous model assumes nanobubbles evenly coat the hydrophobic surface. In reality, the images of Tyrell and Attard<sup>10</sup> indicate that the surface is covered nonuniformly with nanobubbles. In this case, the actual influence of the gas layer is mitigated by regions of liquid–solid interfaces, which produces regions of no slip. Therefore, the actual slip velocity or slip length will be a combination of both regions

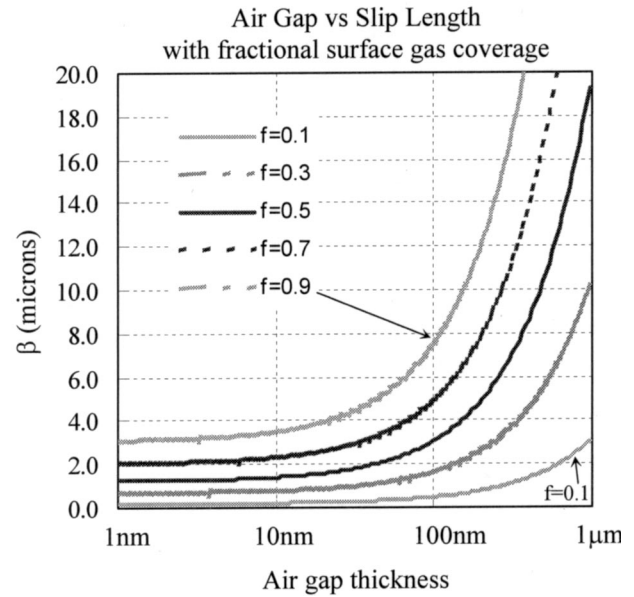


FIG. 5. Air gap versus slip length with fractional surface gas coverage assuming  $\lambda=100$  nm,  $h=30$   $\mu$ m, and standard conditions for air and water at 20 °C. The slip length increases with increasing gas fraction;  $f=0.1$  bottom curve,  $f=0.9$  top curve.

of slip produced by the rarefied gas layer (the nanobubbles) and regions of no slip separating the nanobubbles. We combine the solutions for slip and no slip and determine the degree of surface coverage of gas required to produce experimentally observed slip lengths. Equation (5) provides the velocity profile for water flowing between two infinite parallel plates assuming a rarefied gas layer at the hydrophobic walls. Solving Stokes flow between two infinite parallel plates assuming no slip at the walls and no stress at the centerline yields the velocity equation

$$u_{\text{no-slip}} = \frac{h^2}{2\mu_w} \left( \frac{-dp}{dx} \right) \left[ 1 - \left( \frac{y-h}{h} \right)^2 \right], \tag{7}$$

where each term has been defined previously. We combine the slip and no-slip velocity equations [Eqs. (5) and (7)] in a weighted average and calculate the cumulative velocity,  $u_{\text{cu}}$ , by

$$u_{\text{cu}} = f u_{\text{slip}} + (1-f) u_{\text{no-slip}}, \tag{8}$$

where  $f$  is the surface fraction covered by gas. Assuming Navier’s hypothesis effectively describes the regions of nanobubbles and no slip at the wall, we set the cumulative velocity at the air–water interface equal to the slip length times the shear rate at the air–water interface and obtain an equation for the slip length as a function of plate separation, air gap thickness, and surface fraction of gas

$$\beta_{\text{cu}} = \frac{2f\mu_w \left( \varepsilon\delta + \frac{\delta^2}{2} + (\varepsilon + \delta)h \right)}{\mu_a(2-f)h}. \tag{9}$$

Figure 5 shows the slip length as a function of air gap

thickness (with  $h = 30 \mu\text{m}$ ,  $\lambda = 100 \text{ nm}$ ) for various surface fractions covered with gas. The resulting curves are similar to Fig. 4 where the surface fraction equals 1. For each surface fraction, the slip length rises dramatically as the thickness increases, and eventually exceeds those measured experimentally. At a small air gap thickness (less than  $\sim 10 \text{ nm}$ ), the slip length is nearly constant and increases as the surface fraction of gas increases. The minimum slip length increases from zero at a surface fraction equal to zero ( $f = 0$ , no slip) to a maximum slip length of  $3.68 \mu\text{m}$  at a surface fraction equal to 1. For a slip length of  $\beta = 0.9 \mu\text{m}$  and the approximate nanobubble heights of Tyrell and Attard<sup>10</sup> ( $\delta = 20 \text{ nm}$ ), the experimentally estimated slip length matches the calculated slip length at a surface fraction equal to 0.32. For smaller bubble heights, the required surface fraction increases to  $f = 0.36$  for  $\delta = 10 \text{ nm}$  and  $f = 0.4$  for  $\delta = 1 \text{ nm}$ . These surface fractions are significantly lower than the experimental observations of Tyrell and Attard,<sup>10</sup> where a hydrophobic surface is almost completely covered with nanobubbles.

#### IV. DISCUSSION

Recently, Luaga and Stone<sup>19</sup> analytically examined flow through a pipe with alternating regions of slip and no slip imposed along the walls. Their results are consistent with Tyrell and Attard's<sup>10</sup> observation in that they calculate surface coverage of approximately 97% to produce slip lengths similar to experimentally measured values. In this work, the velocity profiles calculated assume the flow is fully developed over the regions of slip and no slip. In reality, the flow field is constantly developing from regions of slip (nanobubbles) to no slip (spaces between nanobubbles), and vice versa. For the surface coverage calculated, the fully developed assumption overestimates the velocity in the nanobubble regions and increases the cumulative slip length. In addition, the simplified model underestimates viscous dissipation that results from the three-dimensional structure of the nanobubbles and consequently overestimates the effective slip length.

As stated, the nonuniformity of nanobubbles should produce a transient nature to the velocity profile along a hydrophobic surface, with the velocity profile constantly developing from regions of slip (nanobubbles) to no slip (spaces between nanobubbles), and vice versa. The average velocity profiles reported in Tretheway and Meinhart<sup>8</sup> and provided in Fig. 1 result from averaging 16 velocity profiles along the streamwise direction. Thus, any spatially transient nature of the velocity profiles is mitigated. A closer examination of the experimental profiles reveals spatially varying velocity profiles. Figure 6 shows eight velocity profiles along the hydrophobic microchannel wall. These profiles were combined with eight additional profiles and displayed as the average profile in Fig. 1. From Fig. 6, the developing nature of the flow field is observed with the slip velocity at the wall varying from nearly no slip to significant slip. For example, profile (a) exhibits a moderate slip velocity at the wall. As the flow proceeds down the channel, the slip velocity increases to a maximum at profile (b), but then decreases to nearly no

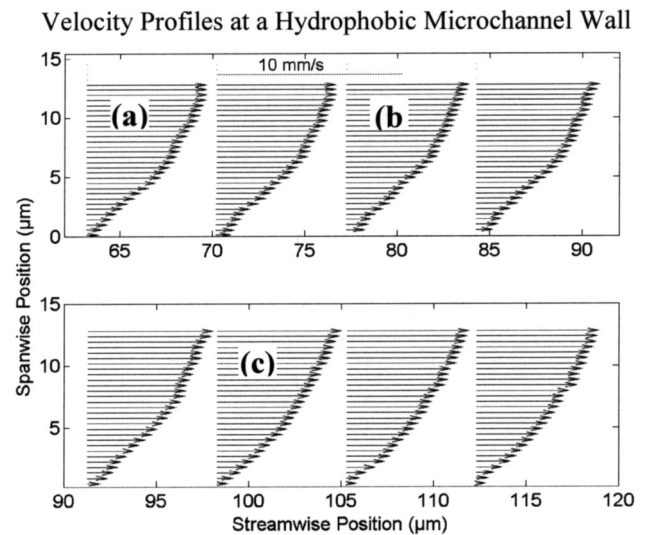


FIG. 6. Velocity profiles along a hydrophobic microchannel wall. The profiles evolve between regions of slip and regions of no slip. Moderate slip at profile (a) increasing to substantial slip at profile (b), then decreasing to nearly no slip at profile (c).

slip at profile (c). This observed variation in slip velocity may develop from regions of high gas surface coverage and low gas surface coverage.

Recently, Choi *et al.*<sup>9</sup> measured pressure drops for flow through hydrophobic and hydrophilic microchannels. From discrepancies with the expected pressure drop, slip lengths of tens of nanometers were calculated for both hydrophilic and hydrophobic surfaces, with hydrophobic surfaces having slightly larger slip lengths. Their slip lengths ( $\beta = 30 \text{ nm}$ ) are substantially smaller than those measured by Tretheway and Meinhart,<sup>8</sup> Pit *et al.*,<sup>4</sup> and Zhu and Granick.<sup>6</sup> We believe this discrepancy may result from differences in the thickness of either nanobubbles at the hydrophobic surface or the depleted layer. The absolute pressure associated with experiments of Tyrell and Attard,<sup>10</sup> Tretheway and Meinhart,<sup>8</sup> Pit *et al.*,<sup>4</sup> and Zhu and Granick<sup>6</sup> are nearly atmospheric. In the experiments of Choi *et al.*,<sup>9</sup> the pressure required to pump fluid through the micron size channels is a few atmospheres. This substantial increase in the pressure may inhibit the formation of nanobubbles and limit their effective height. In addition, the microchannel surfaces were atomically smooth, which may inhibit bubble nucleation. Thus, the slip observed by Choi *et al.*<sup>9</sup> may develop from a mechanism other than that described above. The effect of absolute pressure on the apparent fluid slip is the subject of ongoing investigations.

Several researchers (Zhu and Granick,<sup>6</sup> Craig *et al.*,<sup>5</sup> Choi *et al.*, and others) observe a rate dependence of measured slip lengths. The idealized air gap model cannot be used to directly explain the observed rate dependence. However, the calculated slip lengths encompass the entire range of measured slip lengths, even though the rate dependence is relatively nonuniform. Granick *et al.*<sup>15</sup> and others suggest the rate dependence may develop from an increase in the nucleation of bubbles at higher shear rates. This idea is consistent with Fig. 5. As the nucleation of bubbles increases, the sur-

face bubble coverage increases. Thus, we would expect from Fig. 5 that the slip length increases as the shear rate increases, if the nucleation of bubbles increases. While bubble nucleation and increased surface coverage may explain the slip length shear dependence, details remain elusive.

Finally, modeling nanobubbles or a depleted layer as an effective air gap substantially simplifies a complex three-dimensional problem. In addition, the analytical solutions are obtained for two-dimensional flow between infinite parallel plates, while experimental slip lengths are determined from three-dimensional geometries. Obviously, these simplifications adversely affect the quantitative comparisons between the theoretical and experimental values. However, the results indicate that the presence of a gas layer, depleted region, or nanobubbles at a hydrophobic surface may produce an apparent fluid slip, which is observed experimentally. Detailed numerical simulations are clearly necessary to quantify accurately the effects of either nanobubbles or a depleted water layer and to explore the slip length shear rate dependence.

## V. SUMMARY

An analytical model is developed to quantify the effects an air gap (an idealized case for nanobubbles or a depleted layer) has on fluid flow between two infinite parallel plates. The calculated slip lengths indicate that the presence of nanobubbles or a low viscosity layer may be responsible for the apparent fluid slip observed experimentally by Tretheway and Meinhart,<sup>8</sup> Pit *et al.*,<sup>4</sup> Zhu and Granick,<sup>6</sup> and others. The substantially smaller slip lengths measured by Choi *et al.*<sup>9</sup> suggest that the effects of nanobubbles and hydrophobicity may be significantly reduced at higher absolute pressures and for atomically smooth surfaces. Finally, the simplified nature of the two-dimensional analytical solutions overestimates the fluid slip that develops from rarefied gas conditions. Thus, detailed numerical simulations are necessary to fully understand the effects of hydrophobic surfaces on fluid flow through microchannels.

## ACKNOWLEDGMENTS

This work is supported by NSF CTS-9874839, NSF ACI-0086061, and DARPA/Air Force 30602-00-2-0609.

- <sup>1</sup>E. Ruckenstein and P. Rajora, "On the no-slip boundary condition of hydrodynamics," *J. Colloid Interface Sci.* **96**, 488 (1983).
- <sup>2</sup>J. Barrat and L. Bocquet, "Large slip effect at a nonwetting fluid–solid interface," *Phys. Rev. Lett.* **82**, 4671 (1999).
- <sup>3</sup>N. Churaev, V. Sobolev, and A. Somov, "Slippage of liquids over lyophobic solid surfaces," *J. Colloid Interface Sci.* **97**, 574 (1984).
- <sup>4</sup>R. Pit, H. Hervet, and L. Leger, "Direct experimental evidence of slip in hexadecane: Solid interfaces," *Phys. Rev. Lett.* **85**, 980 (2000).
- <sup>5</sup>V. S. J. Craig, C. Neto, and D. R. M. Williams, "Shear-dependent boundary slip in an aqueous Newtonian liquid," *Phys. Rev. Lett.* **87**, 054504 (2001).
- <sup>6</sup>Y. Zhu and S. Granick, "Rate-dependent slip of Newtonian liquid at smooth surfaces," *Phys. Rev. Lett.* **87**, 096105 (2001).
- <sup>7</sup>Y. Zhu and S. Granick, "Limits of the hydrodynamic no-slip boundary condition," *Phys. Rev. Lett.* **88**, 106102 (2002).
- <sup>8</sup>D. C. Tretheway and C. D. Meinhart, "Apparent fluid slip at hydrophobic microchannel walls," *Phys. Fluids* **14**, L9 (2002).
- <sup>9</sup>C. Choi, J. A. Westin, and K. S. Breuer, "Apparent slip flows in hydrophilic and hydrophobic microchannels," *Phys. Fluids* **15**, 2897 (2003).
- <sup>10</sup>J. Tyrell and P. Attard, "Images of nanobubbles on hydrophobic surfaces and their interactions," *Phys. Rev. Lett.* **87**, 176104 (2001).
- <sup>11</sup>R. Steitz, T. Gutberlet, T. Hauss, B. Klosgen, R. Krastev, S. Schemmel, A. C. Simonsen, and G. H. Findenegg, "Nanobubbles and their precursor layer at the interface of water against a hydrophobic surface," *Langmuir* **19**, 2409 (2003).
- <sup>12</sup>K. Lum, D. Chandler, and J. D. Weeks, "Hydrophobicity at small and large length scales," *J. Phys. Chem. B* **103**, 4570 (1999).
- <sup>13</sup>M. Sakurai, H. Tamagawa, K. Ariga, T. Kunitake, and Y. Inoue, "Molecular dynamics simulation of water between hydrophobic surfaces. Implications for the long-range hydrophobic force," *Chem. Phys. Lett.* **289**, 567 (1998).
- <sup>14</sup>D. Schwendel, T. Hayashi, R. Dahint, A. Pertsin, M. Grunze, R. Steitz, and F. Schreiber, "Interaction of water with self-assembled monolayers: Neutron reflectivity measurements of the water density in the interface region," *Langmuir* **19**, 2284 (2003).
- <sup>15</sup>S. Granick, Y. Zhu, and H. Lee, "Slippery questions about complex fluids flowing past solids," *Nature Mater.* **2**, 221 (2003).
- <sup>16</sup>P. G. de Gennes, "On fluid/wall slippage," *Langmuir* **18**, 3413 (2002).
- <sup>17</sup>C. Meinhart, S. Wereley, and J. Santiago, "A PIV algorithm for estimating time-averaged velocity fields," *J. Fluids Eng.* **122**, 285 (2000).
- <sup>18</sup>T. Gombosi, *Gaskinetic Theory* (Cambridge University Press, Cambridge, 1994), pp. 139–141.
- <sup>19</sup>E. Luaga and H. A. Stone, "Effective slip in pressure driven Stokes flow," *J. Fluid Mech.* **489**, 55 (2003).